

# Modeling of block copolymer dry etching for directed self-assembly lithography

Zelalem Belete\*<sup>a</sup>, Eberhard Baer<sup>b</sup>, Andreas Erdmann<sup>a b</sup>

<sup>a</sup>Friedrich-Alexander-University of Erlangen-Nuremberg, Chair of Electron Devices, Cauerstrasse 6, 91058 Erlangen, Germany

<sup>b</sup>Fraunhofer Institute for Integrated Systems and Device Technology, Schottkystrasse 10, 91058 Erlangen, Germany

## ABSTRACT

Directed self-assembly (DSA) of block copolymers (BCP) is a promising alternative technology to overcome the limits of patterning for the semiconductor industry. DSA exploits the self-assembling property of BCPs for nano-scale manufacturing and to repair defects in patterns created during photolithography. After self-assembly of BCPs, to transfer the created pattern to the underlying substrate, selective etching of PMMA (poly (methyl methacrylate)) to PS (polystyrene) is required. However, the etch process to transfer the self-assembled “fingerprint” DSA patterns to the underlying layer is still a challenge. Using combined experimental and modelling studies increases understanding of plasma interaction with BCP materials during the etch process and supports the development of selective process that form well-defined patterns. In this paper, a simple model based on a generic surface model has been developed and an investigation to understand the etch behavior of PS-b-PMMA for Ar, and Ar/O<sub>2</sub> plasma chemistries has been conducted. The implemented model is calibrated for etch rates and etch profiles with literature data to extract parameters and conduct simulations. In order to understand the effect of the plasma on the block copolymers, first the etch model was calibrated for polystyrene (PS) and poly (methyl methacrylate) (PMMA) homopolymers. After calibration of the model with the homopolymers etch rate, a full Monte-Carlo simulation was conducted and simulation results are compared with the critical-dimension (CD) and selectivity of etch profile measurement. In addition, etch simulations for lamellae pattern have been demonstrated, using the implemented model.

**Keywords:** directed self-assembly (DSA), block copolymers (PS-b-PMMA), plasma etching, modeling, Ar<sup>+</sup> plasma, Ar/O<sub>2</sub> plasma, polystyrene, poly (methyl methacrylate)

\* zelalem.tamrate.belete@leb.eei.uni-erlangen.de; phone 49 9131 761-614; fax 49 9131 85-28698; www.leb.eei.uni-erlangen.de

## 1. INTRODUCTION

Directed self-assembly is a cost-effective alternative approach to EUV lithography, which enables patterning of features below the resolution limit of optical lithography<sup>1</sup>. It uses block copolymers containing two polymers that are micro-phase separated and self-assemble to create structures at nanoscale when annealed<sup>2</sup>. The composition of polystyrene (PS) and poly (methyl methacrylate) (PMMA) in the BCP determines the way they align themselves to form periodic arrays of cylinders, spheres, or lamellae on guiding patterns created by 193 nm immersion lithography or EUV lithography<sup>3</sup>. In order to transfer the pattern created during directed self-assembly onto the underlying layer, the PMMA has to be etched and the remaining PS will be used as a mask for the etching process to follow. As the BCP film thickness is small, high etch selectivity is necessary. Wet etching of BCPs for lamella features results in collapse of features even though it has a very high etch selectivity between PS and PMMA. Plasma dry etching has better control but it is difficult to achieve high selectivity. In addition, due to complex processes occurring in the plasma during etching of polymers, it is difficult to define and control the process easily. Understanding the interaction of polymers with plasmas enables the design of high selectivity and the control of the polymer reactions to the plasma treatment during the etch processes. Several researches have conducted experiments to control the etch selectivity of the polymers by different etch chemistries such as Ar/O<sub>2</sub>, Ar, CO, H<sub>2</sub>, CF<sub>3</sub>, Xe and others<sup>2,4,5</sup>. The difference in etch rate between PS and PMMA arises from the presence of an aromatic ring in PS and of the carbonyl group in PMMA. The chemical structure of PMMA and PS is shown in Figure 1.

In the investigation of the difference in etching behavior of the two polymers using Fourier-transform infrared spectroscopy (FTIR) spectra, the peak intensity of the C=C bond corresponding to the aromatic ring of the PS decreases during the etching process at high bias power stronger than the peak intensity of the C=O bond corresponding to the carbonyl group of the PMMA<sup>6</sup>. This shows that the etching process of PS has a higher etch yield than PMMA. In addition, PMMA is sensitive to sputtering, oxidation and UV radiation and it may spontaneously depolymerize while PS forms a damaged amorphous layer due to cross-link during the etching process. It has to be taken into account that PMMA is rapidly etched during plasma treatment due to its high oxygen content and that the aromatic polymer PS is more resistant to plasma due to its benzene rings<sup>7</sup>.

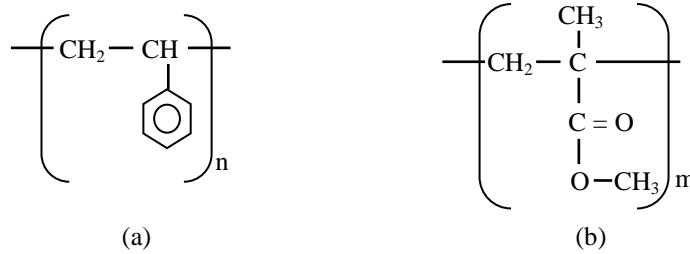


Figure 1. Chemical structure of (a) PS and (b) PMMA

In this paper, modelling of plasma etching for block copolymer, polystyrene-block-poly (methyl methacrylate) (PS-b-PMMA) for different etch chemistries (Ar and Ar/O<sub>2</sub>) is demonstrated. Plasma etching of polymers is a complicated process and a large number of physical and chemical processes occur simultaneously, such as physical sputtering<sup>8</sup>, chemical etching<sup>9</sup>, ion-enhanced chemical etching<sup>8</sup>, cross-linking<sup>10</sup>, chain-scissioning/de-polymerization<sup>11</sup>, and VUV radiation etch<sup>12</sup>. Since it is virtually impossible to include all these phenomena into a model, a simple model that can characterize the final result of the plasma treatment is required accounting for the dominant processes. In order to implement a model that can capture the plasma and polymer interaction for transfer of pattern from DSA to the substrate, the etch behavior of PS and PMMA should be investigated. As a result, first the plasma etching of PMMA and PS homopolymers is studied, to understand the etch behavior of the polymers. For this purpose, we implemented a simple model to compute the etch rate of homopolymers in Ar, and Ar/O<sub>2</sub> plasma. After modeling of the behavior of homopolymers in the plasma, the etching process is simulated for etch profiles for block-copolymer. For the profile simulations, Ar/O<sub>2</sub> plasma etching was selected because this plasma chemistry has a higher selectivity with smaller line-edge-roughness. A simplified model for etching using Ar/O<sub>2</sub> plasma was developed and has been used to simulate etching of selected lamella features. In the model, the sputtering effect of the Ar<sup>+</sup> ions and the ion-enhanced chemical etching by the oxygen neutrals and argon ions are considered, ignoring the effects of oxygen contamination from air exposure. The remaining part of this work is organized as follows: Ar and Ar/O<sub>2</sub> plasma etch chemistries and the corresponding models are presented in Section 2. A procedure for calibration of the models is demonstrated; results are presented and discussed in Section 3. Finally, conclusions are summarized in Section 4.

## 2. MODELING

During plasma treatment of PS and PMMA, hydrogen and oxygen atoms are removed preferentially compared to the carbon atoms. The carbon atoms can cross-link to create a modified layer or be sputtered to etch the polymer.

As reported in literature<sup>13, 14</sup>, surface characterization of Ar<sup>+</sup> irradiation of PMMA for different ion energies using X-ray photoelectron spectroscopy (XPS) spectra for the C 1s region has been carried out. These investigations have shown that pristine PMMA has peaks for C-C, C-O and O-C=O bonds but after Ar<sup>+</sup> plasma treatment the C-O and O-C=O peaks disappear. Similarly, for a CF<sub>3</sub><sup>+</sup> plasma, which modifies the surface not only by physical sputtering but also by ion-enhanced chemical etching, these peaks disappear and showing that the oxygen atoms are etched preferentially. Therefore, during plasma treatment of PMMA, its composition is modified by preferential sputtering of oxygen from the surface<sup>13</sup>. Further plasma treatment can remove the remaining modified PMMA material by physical sputtering or by ion-enhanced chemical etching, depending on the composition of the plasma.

Similarly for PS, as demonstrated by Bruce et al.<sup>10</sup>, during Ar plasma treatment of PS a modified layer with a density different to that of the amorphous carbon is created. This heavily carbon-rich dehydrogenated layer is created by preferential removal of hydrogen atoms from the pristine polymer due to sputtering, ion-induced dehydrogenation and cross-linking<sup>15</sup>.

In order to account for preferential and cascaded etching of the polymers, we assumed a carbon-rich modified and pristine polymer for our model. In this assumption, physical sputtering of the pristine polymer (PS or PMMA) sputters preferentially a fraction of the monomer and the remaining fraction of the monomer cross-links itself. This cross-linking creates a modified layer that has different sputter characteristics to the pristine polymer. The modified layer will subject to the material removal by the different etching mechanisms with different etch rates than those for the pristine polymer.

## 2.1. Etching in a pure Ar plasma

Since Ar neutrals are chemically inert, only physical sputtering is considered for modeling the Ar plasma etching. Furthermore, the effect of etching by VUV radiation is neglected because its effect is small at low temperatures, it only causes densification<sup>10, 16</sup>. Based on these assumptions, a simple model based on surface site balance using Monte-Carlo is implemented.

The etch rate of materials during plasma treatment is proportional to etch yield, the flux of etching species and the atomic density of the materials. The etch yield represents the number of sputtered atoms per incoming etching ion, and it applies to all types of ion bombardment process. For physical sputtering, it can be approximated by<sup>17</sup>

$$Y(E, \phi) = A * (\sqrt{E} - \sqrt{E_{th}}) * f(\phi) \quad (1)$$

where A represents the etch yield constant,  $E_{th}$  is the energy threshold for sputtering, E is the energy of the incident ion, and  $f(\phi)$  determines the angular dependence of the yield, where  $\phi$  is the angle of incidence with respect to the normal of the surface. The angular dependence will be considered for profile simulations while for the etch rate of the homopolymer normal incidence is considered and the angular dependence is neglected. E is calculated from the bias voltage ( $V_{bias}$ ) and the plasma potential ( $V_p$ ) as  $E = (V_{bias} - V_p) * e$ , where e is the elementary charge<sup>18</sup>.

Considering only the surface of the etched material, the balance equation for surface coverage of the cross-linked modified polymer is determined by<sup>19, 20</sup>

$$\frac{d\Theta_p}{dt} = \frac{1}{\sigma} * (\Gamma_i * Y_{cl} * (1.0 - \Theta_p) - \Gamma_i * Y_p * \Theta_p) \quad (2)$$

where  $\Gamma_i$  is the ion flux,  $\Theta_p$  is the coverage of the cross-linked surface,  $\sigma$  is the surface density for PS/PMMA, and  $Y_{cl}$  and  $Y_p$  are the cross-linking yield and the sputter yield for cross-linked polymer, respectively. The first term in Equation (2) is the cross-linking rate, which is dependent on the ion flux and the free surface sites not covered by the cross-linked layer. The second term is the sputter rate of this modified cross linked layer.

Assuming pseudo-steady-state conditions, the surface coverage of the cross-linked polymer can be written as

$$\frac{d\Theta_p}{dt} = 0 \rightarrow \Theta_p = \frac{Y_{cl}}{Y_{cl} + Y_p} \quad (3)$$

During etching by Ar plasma since physical sputtering is the dominant process, the etch rate is determined by the sputtering of pristine and cross-linked layer. It can be calculated by

$$ER = \frac{1}{\rho} * (\Gamma_i * Y_s * (1 - \theta_p) + \Gamma_i * Y_p * \Theta_p) \quad (4)$$

using  $\Theta_p$  from Equation (3). Here  $\rho$  is the number density of PS/PMMA and  $Y_s$  is the sputter yield of the original polymer for PS/PMMA.

## 2.2. Etching in Ar/O<sub>2</sub> plasma

During the Ar/O<sub>2</sub> plasma etch process, due to the presence of reactive neutral oxygen atoms in the plasma, in addition to physical sputtering, chemical etching and ion-enhanced chemical etching occur. In XPS and Raman spectroscopy during plasma treatment of PMMA by O<sub>2</sub> or Ar, the formation of the cross-linked layer was demonstrated<sup>21, 8, 14</sup>. The difference between the two plasma treatments occurs as the duration of the plasma treatment increases: In Ar plasma treatment the fraction of the cross-linked layer increases with time but for an O<sub>2</sub> plasma the cross-linked layer disappears during the treatment, which is due to the oxidation of this modified layer<sup>14</sup>. Additionally, in an Ar/O<sub>2</sub> plasma, the fraction of the cross-linked layer increases as the fraction of Ar in the Ar-O<sub>2</sub> mixture increases. This can be explained by the increased sputtering by Ar before cross linking. As a result, in the model we can calculate the cross-linking as in Equation (2) (which is for pure Ar plasma without chemical reactions) which means that we neglect the effect of ion-enhanced chemical etching as a step before cross-linking.

For the argon plasma, the fraction of the modified cross-linked layer decreases with increasing energy of the ions, as the sputtering of the cross-linked layer is enhanced and dominates over the cross-linking yield.

For O<sub>2</sub> plasma chemistry, Gokan et al.<sup>8</sup> demonstrated that during sputtering of carbon atoms in PMMA, physical sputtering, chemical sputtering (reaction of O<sub>2</sub><sup>+</sup> ions with C) and ion-enhanced chemical etching occur to create H<sub>2</sub>, CO, and CO<sub>2</sub> dominant etch products. During bombardment of polymers with reactive ion species, chemical reactions can take place with the polymer to form molecules locally (chemical sputtering). Then they diffuse to the surface and desorb to etch the surface or they may form loosely bound molecules that can be sputtered easily. In addition, ions can bombard the polymer to create radical sites where neutrals atoms/molecules adsorb to create a volatile product.

In order to model etching in an Ar/O<sub>2</sub> plasma, it is assumed that the cross-linked layer is produced by sputtering of the pristine polymer by Ar<sup>+</sup> and chemical sputtering by O<sub>2</sub><sup>+</sup> ions. It is etched by ion-enhanced chemical etching by oxygen neutral species and physical and chemical sputtering by ions. The pristine polymer is etched by physical sputtering and ion-enhanced chemical etching. In order to model the etching of PMMA and PS in Ar/O<sub>2</sub> plasma chemistry with balance equations, we introduce coverages<sup>22</sup> as described below. For these surface coverages, we consider the fraction of the cross-linked surface as coverage  $\Theta_p$ , the coverage of oxygen on the pristine polymer  $\Theta_o$ , and the coverage of oxygen on the cross-linked layer  $\Theta_{po}$ .

The rate of change of coverage of the cross-linking polymer on the surface is given as

$$\frac{d\Theta_p}{dt} = \frac{1}{\sigma} * (\Gamma_i * Y_{cl} * (1.0 - \Theta_p - \Theta_o) - \Gamma_i * Y_p * (1.0 - \Theta_{po}) * \Theta_p - \Gamma_i * Y_{po} * \Theta_{po} * \Theta_p) \quad (5)$$

where  $Y_{cl}$  is the cross-linking yield,  $Y_p$  is the physical sputter yield and  $Y_{po}$  is the ion-enhanced chemical etching yield of the cross-linked polymer.

The first term in Equation (5) represents the cross-linking yield during sputtering of the pristine polymer, while the second and third term show etching of the cross-linked layer by physical sputtering and ion-enhanced chemical etching, respectively.

Similarly, the rate of change of surface coverage of oxygen atoms on the pristine polymer given as

$$\frac{d\Theta_o}{dt} = \frac{1}{\sigma} * (\Gamma_o * S_o * (1.0 - \Theta_p - \Theta_o) - \Gamma_i * Y_o * \Theta_o) \quad (6)$$

where  $Y_o$  is the yield for the ion-enhanced chemical etching of carbon.

In Equation (6) above, the first term represents the Langmuir-type adsorption on the pristine polymer surface which is proportional to the flux of neutral oxygen atoms ( $\Gamma_o = 2 * \Gamma_{O_2}$ ), their sticking probability ( $S_o$ , which is assumed to be unity<sup>8</sup>) and the fraction of free surface sites not covered by oxygen or the cross-linked polymer. The second term describes the etching of carbon atoms by ion-enhanced chemical etching.

As the cross-linked layer is etched with oxygen neutral species, the coverage of oxygen on this layer is determined by the adsorption of oxygen (first term in Equation (7)) and etching of these adsorbed oxygens by ion enhanced chemical etching (second term of Equation (7)):

$$\frac{d\Theta_{po}}{dt} = \frac{1}{\sigma} * (\Gamma_o * S_{po} * (1.0 - \Theta_{po}) * \Theta_p - \Gamma_i * Y_{po} * \Theta_{po} * \Theta_p) \quad (7)$$

$S_{po}$  is the sticking coefficient of oxygen neutrals on the surface of modified polymer.

Assuming a pseudo-steady-state for the surface coverages,  $\Theta_p$ ,  $\Theta_o$ , and  $\Theta_{po}$ , where  $\frac{d\Theta_i}{dt} = 0$ , leads to

$$\Theta_{po} = \frac{\Gamma_o * S_{po}}{\Gamma_o * S_{op} + \Gamma_i * Y_{po}} \quad (8)$$

$$\Theta_o = \frac{\Gamma_o * S_o * (1.0 - \Theta_p)}{\Gamma_o * S_o + \Gamma_i * Y_o} \quad (9)$$

$$\Theta_p = \frac{\Gamma_i * Y_{cl} * (1.0 - \Theta_o)}{\Gamma_i * Y_{cl} + \Gamma_o * Y_{po} * \Theta_{po} + \Gamma_i * Y_p * (1.0 - \Theta_{po})} \quad (10)$$

where  $\Theta_p$ ,  $\Theta_o$ , and  $\Theta_{po}$  have a value between 0.0 and 1.0.  $\Theta_p = 0$  means there is no cross-linked layer in the process (at the beginning of the process) or the cross-linked (modified) layer is etched completely during the process, while  $\Theta_p = 1$  represents the pristine polymer surface being completely cross-linked.

The etch rate is determined by physical sputtering and ion-enhanced chemical etching, assuming the cross-linking process does not have a deposition effect during etching apart from modifying the property of the surface. After calculation of the surface coverages from neutral and ion flux, the local etch rate is calculated by.

$$ER = \frac{1}{\rho} * (\Gamma_i * Y_s * (1 - \Theta_p - \Theta_o) + \Gamma_i * Y_o * \Theta_o + \Gamma_i * Y_p * (1 - \Theta_{po}) * \Theta_p + \Gamma_i * Y_{po} * \Theta_{po} * \Theta_p) \quad (11)$$

where  $Y_s$  is the sputter yield of the pristine PMMA/PS polymer and  $\rho$  is the bulk carbon number density ( $2.36 * 10^{21} \text{ cm}^{-3}$  for PMMA and  $7.5 * 10^{20} \text{ cm}^{-3}$  for PS).

The first term in the etch rate calculation represents the physical sputtering of the pristine polymer and depends on the total ion flux and the surface sites free from oxygen coverage and cross-linking. The second term accounts for oxygen ion-enhanced chemical etching of the pristine polymer, while the third and fourth term represent etching of the cross-linked layer by physical sputtering and by ion-enhanced chemical etching, respectively.

### 3. MODEL CALIBRATION

#### 3.1. Etching in pure Ar plasma

In order to extract model parameters, the models have to be calibrated with experimental or literature data. Calibration data for etching was extracted from Ting et al.<sup>23</sup>, where the etch rate of PMMA and PS homopolymers was measured for Ar, O<sub>2</sub>, Ar/O<sub>2</sub> plasmas at different bias voltages (ion energies). For the calibration we used Pythmea<sup>24</sup>, which is a multi-objective optimizer from Dr.LiTHO<sup>25</sup>.

Ting et al.<sup>23</sup> used a helicon plasma etcher for etching of the polymers, which has a decoupled plasma source power and self-bias power to enable variation of ion energy by changing the bias voltage independent of ion flux<sup>23</sup>. A constant ion flux and different ion energies were used to calibrate the homopolymers etch rate. Cumpson et al.<sup>26</sup> developed a sputtering model for Ar<sup>+</sup> ions and fitted the experimental data to determine the sputter yield dependence on the ion energy for different materials. They estimated the sputter threshold energy of PMMA and PS to be 2.25 eV and 2.20 eV respectively. We used these values to fit our model with the measured etch rate values.

The formation of the cross-linked layer during Ar plasma etch was demonstrated by Liu et al.<sup>27</sup>. After Ar plasma treatment, the solubility of the PS was changed, which shows the formation of a cross-linked layer. But for our model, we were able to get comparable fitting results for calibrations with cross-linking process or without cross-linking process during plasma treatment. As a result, we calibrated the model without cross-linking process during etching. This can be explained by the fact that even though there is a formation of cross-linked layer, it does not impact the etch behavior of the polymers. Due to the low flux of Ar<sup>+</sup> ions in the plasma, the formation of cross-linked layer is not strong enough to change the etch behavior of the polymers.

In order to calibrate the model without cross-linking layer formation, parameters  $Y_{cl}$ ,  $Y_p$ ,  $\theta_p$  are set to zero in Equations (2), (3), and (4).

The calibration results are shown in Table 1. In Figure 2, we show a comparison of the simulated and measured ion energy dependence of the etch rate. The simulated curves have been generated using the parameter values shown in Table 1 and the etch rate has been determined according to Equation (4). The calibrations of the model for Ar etch chemistry have root-mean-squared error (RMSE) of 2.65 nm/min for PS and 12.96 nm/min for PMMA.

Table 1. Model parameter values determined from calibration for Ar plasma etch

parameters	range	value
PS sputter yield constant, $A_{PS}$	$10^{-6} - 10^0$	$1.34 \cdot 10^{-5}$
PMMA sputter yield constant, $A_{PMMA}$	$10^{-6} - 10^0$	$1.75 \cdot 10^{-4}$

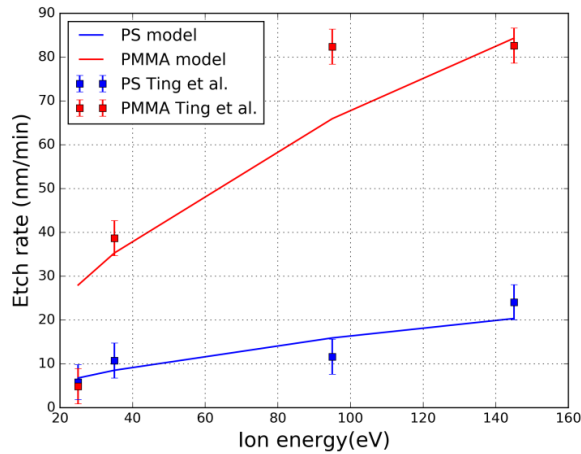


Figure 2. Ar plasma etch model calibration for Ting et al.<sup>23</sup> etch rate measurement

### 3.2. Etching in Ar/O<sub>2</sub> plasma

In order to simulate the effect of O<sub>2</sub> in the Ar plasma, an additional coverage for oxygen is added in the model in Equations (6), (7), and (8). The cross-linked polymer will be etched by ion-enhanced chemical etching and sputter

etching and the pristine will be etched by chemical etching and ion enhanced chemical etching and defined in the model by Equation (11).

The ion-enhanced chemical etching yield energy threshold for the pristine PS and PMMA layer is assumed to be two times the minimum energy required to break the C-C bond. This is due to the reason that two covalent C-C bonds have to be broken to enable the oxygens adsorbed on the pristine surface to produce volatile etch product, CO, and desorb to etch the carbon atoms<sup>26, 8</sup>. In literature, for the minimum energy required to break the C-C bond, a value of 5 eV is reported<sup>28</sup>. Similar to Ar plasma model calibration, the effect of cross-linking for PMMA and PS is ignored. As a result, parameters  $Y_{cl}$ ,  $Y_p$ ,  $\theta_p$ ,  $Y_{po}$ ,  $Y_o$ ,  $\theta_{po}$  are set to be zero in Equations (5), (6), (7), (8), (9), (10), and (11).

Due to the small flow of oxygen for etching of the polymers in Ting et al. and large number of carbon atoms contained in PS the sticking coefficient ( $S_o$ ) is assumed 1.0. The sticking probability of oxygen on PMMA is lower than on PS, due to oxygen already contained in the monomer. Gokan et al.<sup>8</sup> reported 38% of the incoming  $O_2$  recoil from the PMMA surface. As a result, sticking coefficient ( $S_o$ ) for PMMA is assumed to 0.6.

In addition to physical sputtering, oxygen ions ( $O_2^+$  and  $O^+$ ) in the Ar/ $O_2$  plasma produce volatile etch products, CO and  $CO_2$  at low ion energies<sup>29, 8</sup>. We assumed the contribution of chemical sputtering to the etch rate to be negligible compared to physical sputtering. Therefore, we calibrated the Ar/ $O_2$  etch model using sputtering parameters calibrated for the Ar plasma.

The parameters calibrated for Ar/ $O_2$  model are shown in Table 2. The ion-enhanced chemical etching yield ( $Y_o$ ) constants  $A_{o,PS}$  (for PS) and  $A_{o,PMMA}$  (for PMMA), and the oxygen flux ( $\Gamma_o$ ) are calibrated with the literature data. Figure 3, shows the comparison for the simulated and measured ion energy dependence of the etch rate. The simulated curves are generated using the parameter values shown in Table 2 and Table 1 and the etch rate has been determined according to Equation (11). The calibrations of the model for Ar/ $O_2$  etch chemistry have root-mean-squared error (RMSE) of 12.7 nm/min for PS and 21.8 nm/min for PMMA.

Table 2. Model parameter values determined from calibration for Ar/ $O_2$  plasma etch

parameters	Range	Fitted values
Oxygen flux, $\Gamma_o$ ( $cm^{-2}s^{-1}$ )	$10^{16} - 10^{19}$	$5.84 \cdot 10^{17}$
PS oxygen yield ( $Y_o$ ) constant, $A_{o,PS}$	$10^{-6} - 10^0$	$1.46 \cdot 10^{-3}$
PMMA oxygen yield ( $Y_o$ ) constant, $A_{o,PMMA}$	$10^{-6} - 10^0$	$8.5 \cdot 10^{-3}$

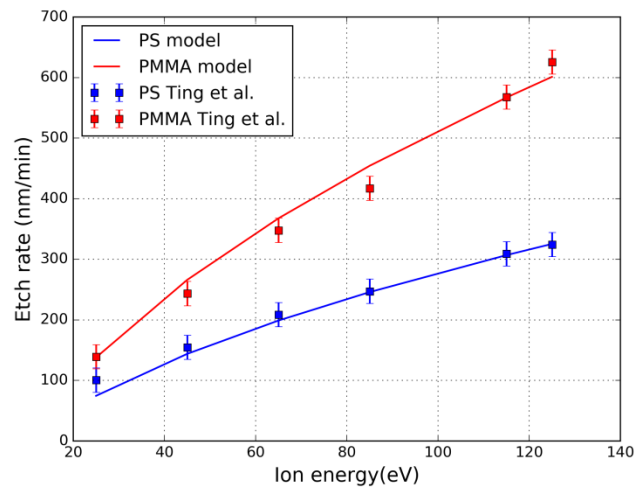


Figure 3. Ar/ $O_2$  plasma etch model calibration for Ting et al.<sup>23</sup> etch rate measurement

As it can be seen from the comparison plot in Figure 3, the model shows good agreement with the measured energy dependence of etch rate.

### 3.3. Profile simulation for Ar/O<sub>2</sub> plasma

In order to simulate the etch profile of a DSA lamella or a contact hole shrink, the angular dependence of sputtering and chemical enhanced etching has to be included in the model. The angular dependence for sputter yield and ion-enhanced chemical etch yield,  $f(\phi)$  can be approximated by simple polynomial equations<sup>16, 19, 30</sup>, where  $\phi$  is the angle of ion incidence with respect to the normal to the surface. For physical sputtering, the yield has a maximum at an off-normal angle  $\beta$  and declines to zero at  $\frac{\pi}{2}$ , as shown in Figure 4<sup>30, 31</sup>.

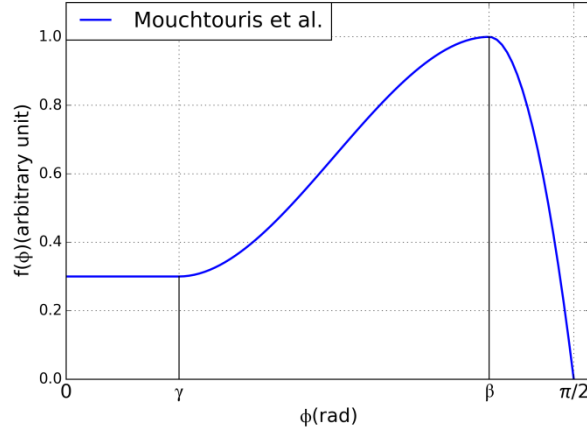


Figure 4. Ion incidence angle dependence of physical sputtering yield of PMMA by Ar<sup>+</sup> ions<sup>16</sup>

The polynomial approximation for the angular dependence for the sputtering yield by Ar<sup>+</sup> ions for PMMA is show below in Equation (12), taken from Mouchtouris et al.<sup>16</sup>.

$$f(\phi) = \begin{cases} a, & \phi < \gamma \\ b_0 + b_1\phi + b_2\phi^2 + b_3\phi^3, & \gamma < \phi < \beta \\ 1 + c(\phi - \beta), & \phi \geq \beta \end{cases} \quad (12)$$

$a$ ,  $\gamma$  (in radians), and  $\beta$  (in radians) are the ratio of normal incidence angle sputter yield over maximum sputter yield, the angle below which the sputter yield is constant, and the angle corresponding to the maximum sputter yield respectively. The values are;  $a = 0.3$ ,  $\gamma = 20^\circ$  and  $\beta = 75^\circ$ .

The parameters  $b_3$ ,  $b_2$ ,  $b_1$ ,  $b_0$  and  $c$  are calculated by

$$c = \frac{a - 1}{3\gamma\beta(\gamma - \beta) - 1.5(\gamma + \beta)(\gamma^2 - \beta^2)(\gamma^3 - \beta^3)} \quad (13)$$

$$b_1 = 1.5(\gamma + \beta)b_3 \quad (14)$$

$$b_2 = 3b_1\gamma\beta \quad (15)$$

$$b_0 = 1 - b_1\beta - b_2\beta^2 - b_3\beta^3 \quad (16)$$

$$c = \frac{1}{(\pi/2 - \beta)^2} \quad (17)$$

Due to the absence of data on the angular dependence of the sputter yield of PS we assumed that the angular dependence (normalized curve) of PS is the same as for PMMA. For the absolute value of the sputter yields of PS and PMMA, the measured selectivity between sputter etching of PMMA versus PS (determined by lamella etching and homopolymer etching, Ting et al.<sup>23</sup>) is taken into account. The angular dependence of ion-enhanced chemical etching yield by O<sub>2</sub> and Ar<sup>+</sup> ions was assumed to have no angular dependence.

A full Monte-Carlo simulation for Ar/O<sub>2</sub> plasma chemistry was performed for a BCP lamella structure with 80 nm thickness and 25 nm CD, shown in Figure 5. The simulation takes into account the sputter yield angular dependence and a single lamella was considered. For profile simulation, after the etch rates for PMMA and PS surfaces have been calculated, the surface is updated with the corresponding etch rates and the etch rates are recalculated for the new surface. The etch rates were calculated using the calibrated values in Table 1 and 2 and using Equation (11). A level set method<sup>32</sup> is used to update the surface, as this method is robust and handles deformation, merging or separation of surfaces naturally.

The final etch results were in agreement with the etch selectivity and remaining PS CD measurements reported in Ting et al.<sup>23</sup>. The final etched profile has a CD of 24.24 nm and a selectivity of 2.04 from literature<sup>23</sup>. The simulated final remaining PS profile has a CD of 24.86 nm and an etch selectivity of 1.85.

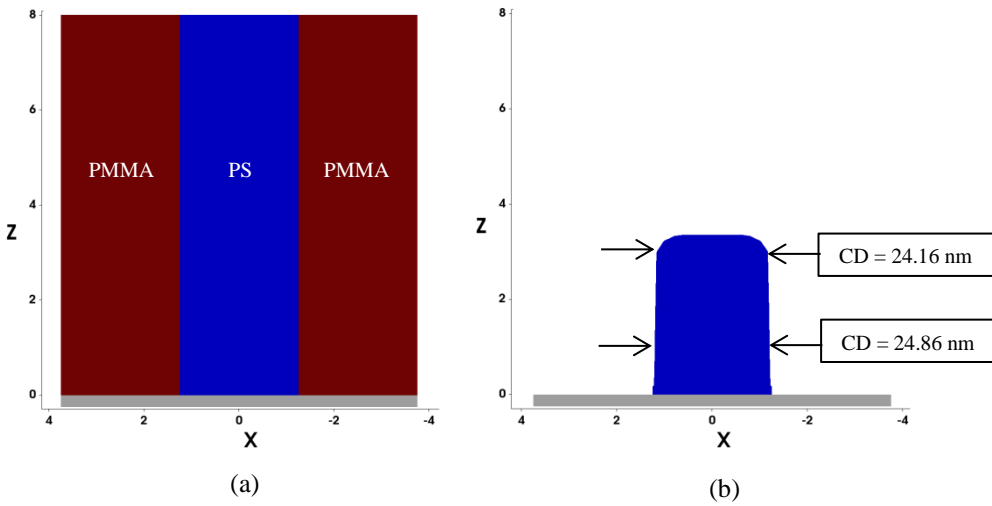


Figure 5. Ar/O<sub>2</sub> plasma etch for lamella structure, (a) initial geometry, blue region represents PS and red region represents PMMA (b) etched profile for an ion energy of 125 eV and with 110 % of the time required to etch PMMA homopolymer with thickness of 80 nm. The plots are scaled by 0.1 nm.

In order to demonstrate the application of the model for etching of directed self-assembly of BCP, we have conducted simulations for contact-hole shrink and lamellae features. For a contact hole shrink pattern, a feature where the bottom and side of the guiding pattern has affinity for PS was simulated by Ohta-Kawasaki model using DSA assembly simulator module Dr.Seal from Dr.LiTHO<sup>25</sup>. The contact hole was etched using 115 eV ion energy and the etched profile at different time steps is shown in Figure 6. The photoresist guiding pattern for the contact-hole is assumed to be not etched during the treatment. This can result in a shadowing effect on the profile during etch simulation.

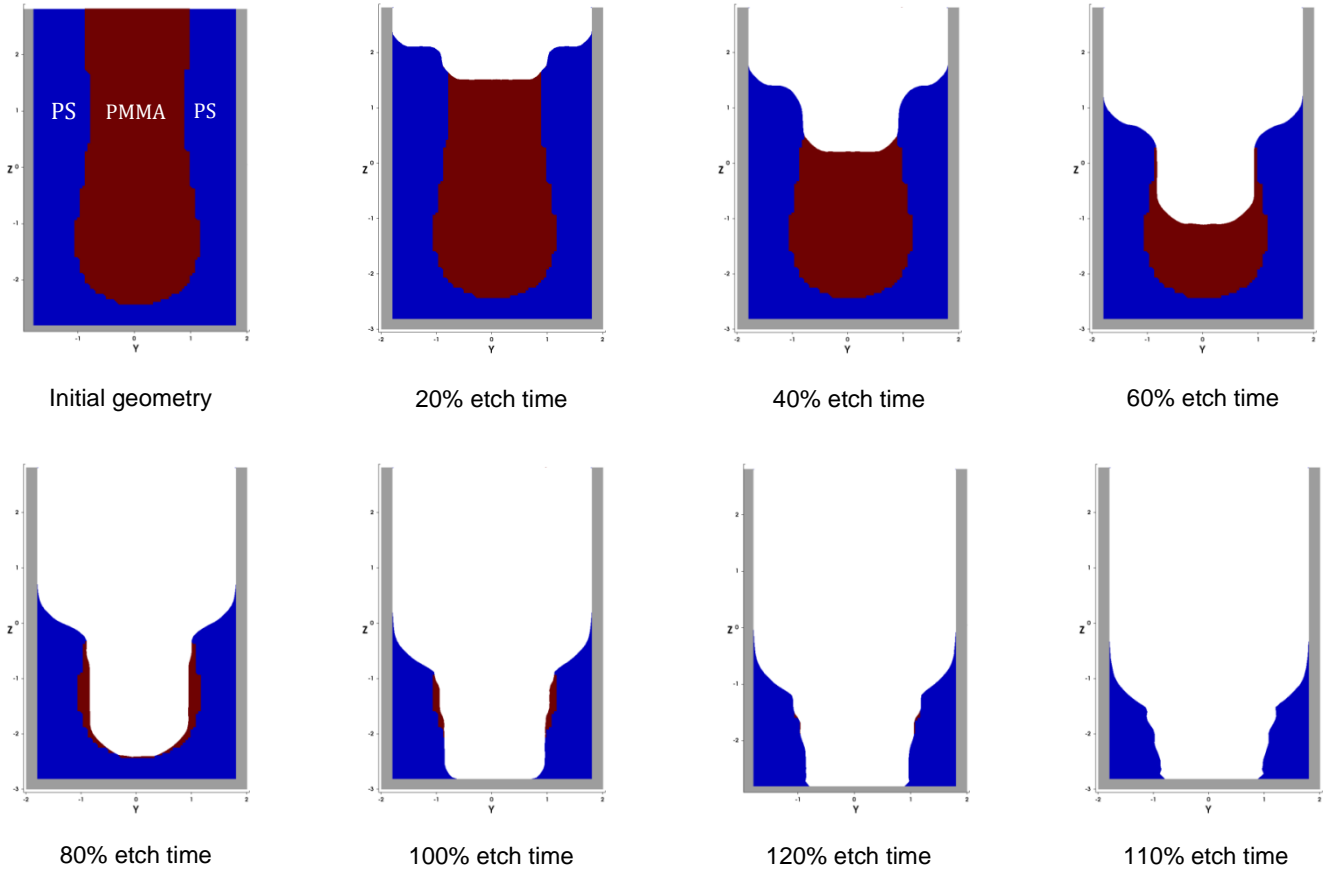


Figure 6. Etch profiles at time steps for 115 eV ion energy, percentage etch time is the etch time normalized with time until PS is etched through in the center (that is after etching of 52.93 nm PMMA and 5.6 nm PS). The initial structure generated by self-assembly of block copolymers was simulated with Dr.LiTHO<sup>26</sup>. The plots are scaled by 0.1 nm.

#### 4. CONCLUSION AND FUTURE WORK

An etch model for etching of DSA patterns for Ar and Ar/O<sub>2</sub> plasma chemistries has been demonstrated. The effect of the cross-linked layer on the etch behavior of the polymers was investigated. The model was able to reproduce measurements from literature data with reasonable accuracy without the inclusion of the cross-linked layer formation. This can be explained by the fact that due to the small flux of Ar<sup>+</sup> ions, the effect of cross-linked layer on etch rate is small. The result agrees with the observations of Choudhary et al.<sup>33</sup>, where polymers have high sputter yield for small flux of ions and small sputter yield at high ion fluxes. For high flux of ions, the formation of the cross-linked layer formation increases and changes the behavior of the polymer to be etch resistant. The fact that the model was able to fit with the literature data without inclusion of cross-linking layer formation shows that the etch behavior of the polymers is not changed due to small flux of ions. The etch rates of the PS and PMMA homopolymers etch rate can be approximated by a model. Monte-Carlo based profile etch simulations for self-assembled block copolymer fingerprint patterns have been conducted. Profile simulations using model parameters extracted by fitting the model with homopolymer etch rates give results which agree with literature data. The model was able to reproduce the measured CD and thicknesses of the remaining PS profiles, by including the angular dependence of the etch yield in the model. Comprehensive data for the process steps in the etching of these polymers is rarely reported. Due to the lack of literature data with full and detailed description of the process, we are limited with respect to the calibration of the model. Due to assumptions for the calibration of the model, the accuracy and the effect of some parameter can be diminished or exaggerated. Further

investigations based on additional experimental data can give a better understanding of the etch processes. In addition, the effect of VUV, chemical etching and cross-linking processes on the etch rate can be investigated.

All the simulations are performed using ViennaTS topography simulator level-set engine<sup>32</sup> to update the surface with the corresponding etch rate and Dr.LiTHO<sup>25</sup> to simulate the assembly of block copolymers and to calibrate the simulation parameters for the model.

## ACKNOWLEDGMENTS

The research leading to these results has received funding from the European Union's Horizon 2020 research and innovation programme under grant agreement No 688101 SUPERAID7.

## 5. REFERENCES

- [1] Chan, B. T., Tahara, S., Parnell, D., Rincon Delgadillo, P. A., Gronheid, R., Marneffe, J.-F. de, Xu, K., Nishimura, E. and Boullart, W., "28nm pitch of line/space pattern transfer into silicon substrates with chemo-epitaxy Directed Self-Assembly (DSA) process flow," *Microelectronic Engineering* 123, 180–186 (2014).
- [2] Sarrazin, A., Posseme, N., Pimenta-Barros, P., Barnola, S., Gharbi, A., Argoud, M., Tiron, R. and Cardinaud, C., "PMMA removal selectivity to polystyrene using dry etch approach," *Journal of Vacuum Science & Technology B, Nanotechnology and Microelectronics: Materials, Processing, Measurement, and Phenomena* 34(6), 61802 (2016).
- [3] Jeong, S.-J., Kim, J. Y., Kim, B. H., Moon, H.-S. and Kim, S. O., "Directed self-assembly of block copolymers for next generation nanolithography," *Materials Today* 16(12), 468–476 (2013).
- [4] Omura, M., Imamura, T., Yamamoto, H., Sakai, I. and Hayashi, H., "Highly selective etch gas chemistry design for precise DSAL dry development process," *SPIE Proceedings*, 905409 (2014).
- [5] Tiron, R., Chevalier, X., Gaugiran, S., Pradelles, J., Fontaine, H., Couderc, C., Pain, L., Navarro, C., Chevolleau, T., Cunge, G., Delalande, M., Fleury, G. and Hadziioannou, G., "Pattern density multiplication by direct self assembly of block copolymers: toward 300mm CMOS requirements," *SPIE Proceedings*, 832300-832300-7 (2012).
- [6] Yamamoto, H., Imamura, T., Omura, M., Sakai, I. and Hayashi, H., "Selective etch of poly(methyl methacrylate) in block copolymer based on control of ion energy and design of gas chemistry for directed self assembly lithography," *Jpn. J. Appl. Phys.* 53(3S2), 03DD03 (2014).
- [7] S. Moss, A. Jolly, B. Tighe, "Plasma oxidation of polymers," *Plasma Chem Plasma Process* 6(4), 401–416 (1986).
- [8] H. Gokan and S. Esho, "Sputtering Yield of Carbon Atoms in Organic Materials for Oxygen Bombardment," *Journal of Electrochemical Society: Solid-State science and Technology* 131(5), 1105–1110 (1984).
- [9] Lock, E. H., Petrovykh, D. Y., Mack, P., Carney, T., White, R. G., Walton, S. G. and Fernsler, R. F., "Surface composition, chemistry, and structure of polystyrene modified by electron-beam-generated plasma," *Langmuir : the ACS journal of surfaces and colloids* 26(11), 8857–8868 (2010).
- [10] Bruce, R. L., Engelmann, S., Lin, T., Kwon, T., Phaneuf, R. J., Oehrlein, G. S., Long, B. K., Willson, C. G., Végh, J. J., Nest, D., Graves, D. B. and Alizadeh, A., "Study of ion and vacuum ultraviolet-induced effects on styrene- and ester-based polymers exposed to argon plasma," *J. Vac. Sci. Technol. B* 27(3), 1142 (2009).
- [11] Raudino, A., Fragalà, M. E., Compagnini, G. and Puglisi, O., "Modeling of low-temperature depolymerization of poly (methyl methacrylate) promoted by ion beam," *The Journal of Chemical Physics* 111(4), 1721–1731 (1999).
- [12] Lock, E. H., Walton, S. G. and Fernsler, R. F., "Physio-Chemical Modifications of Polystyrene and Poly(propylene) Surfaces by Electron Beam-Generated Plasmas Produced in Argon," *Plasma Process. Polym.* 6(4), 234–245 (2009).
- [13] Yoshimura, S., Tsukazaki, Y., Kiuchi, M., Sugimoto, S. and Hamaguchi, S., "Sputtering yields and surface modification of poly(methyl methacrylate) (PMMA) by low-energy Ar + /  $\text{CF}_3^+$  ion bombardment with vacuum ultraviolet (VUV) photon irradiation," *J. Phys. D: Appl. Phys.* 45(50), 505201 (2012).
- [14] Dai, W., Ko, T.-J., Oh, K. H., Lee, K.-R. and Moon, M.-W., "Ion-Beam Induced Surface Roughening of Poly-(methyl methacrylate) (PMMA) Tuned by a Mixture of Ar and O<sub>2</sub> Ions," *Plasma Processes Polym.* 9(10), 975–983 (2012).

- [15] Végh, J. J., Nest, D., Graves, D. B., Bruce, R., Engelmann, S., Kwon, T., Phaneuf, R. J., Oehrlein, G. S., Long, B. K. and Willson, C. G., “Near-surface modification of polystyrene by Ar<sup>+</sup>. Molecular dynamics simulations and experimental validation,” *Appl. Phys. Lett.* 91(23), 233113 (2007).
- [16] Mouchtouris, S., “Multiscale Modeling of Low Pressure Plasma Etching Processes: Linking the Operating Parameters of the Plasma Reactor with Surface Roughness Evolution,” *Plasma Process. Polym.* 14 (2017).
- [17] Steinbrüchel, C., “Universal energy dependence of physical and ion-enhanced chemical etch yields at low ion energy,” *Appl. Phys. Lett.* 55(19), 1960–1962 (1989).
- [18] Ting, Y.-H., Liu, C.-C., Park, S.-M., Jiang, H., Nealey, P. F. and Wendt, A. E., “Surface Roughening of Polystyrene and Poly(methyl methacrylate) in Ar/O<sub>2</sub> Plasma Etching,” *Polymers* 2(4), 649–663 (2010).
- [19] Belen, R. J., Gomez, S., Cooperberg, D., Kiehlbauch, M. and Aydil, E. S., “Feature-scale model of Si etching in SF<sub>6</sub>/O<sub>2</sub> plasma and comparison with experiments,” *Journal of Vacuum Science & Technology A: Vacuum, Surfaces, and Films* 23(5), 1430–1439 (2005).
- [20] Große-Kreul, S., Corbella, C., Keudell, A. von, Ozkaya, B. and Grundmeier, G., “Surface Modification of Polypropylene (PP) by Argon Ions and UV Photons,” *Plasma Process. Polym.* 10(12), 1110–1119 (2013).
- [21] Vesel, A. and Mozetic, M., “Surface modification and ageing of PMMA polymer by oxygen plasma treatment,” *Vacuum* 86(6), 634–637 (2012).
- [22] Gogolides, E., “Etching of SiO<sub>2</sub> and Si in fluorocarbon plasmas: A detailed surface model accounting for etching and deposition,” *Journal of Applied Physics* 88(10) (2000).
- [23] Ting, Y.-H., Park, S.-M., Liu, C.-C., Liu, X., Himpsel, F. J., Nealey, P. F. and Wendt, A. E., “Plasma etch removal of poly(methyl methacrylate) in block copolymer lithography,” *J. Vac. Sci. Technol. B* 26(5), 1684 (2008).
- [24] Raidl, G. R., Cagnoni, S., Branke, J., Corne, D. W., Drechsler, R., Jin, Y., Johnson, C. G., Machado, P., Marchiori, E., Rothlauf, F., Smith, G. D., Squillero, G., Fühner, T., Erdmann, A., Farkas, R., Tollkühn, B. and Kókai, G. (eds.), [Genetic Algorithms to Improve Mask and Illumination Geometries in Lithographic Imaging Systems. Applications of Evolutionary Computing], Springer Berlin Heidelberg (2004).
- [25] Fühner, T., Schnattinger, T., Ardelean, G. and Erdmann, A., “Dr.LiTHO: a development and research lithography simulator,” *SPIE Proceedings*, 65203F (2007).
- [26] Cumpson, P. J., Portoles, J. F., Barlow, A. J. and Sano, N., “Accurate argon cluster-ion sputter yields. Measured yields and effect of the sputter threshold in practical depth-profiling by x-ray photoelectron spectroscopy and secondary ion mass spectrometry,” *Journal of Applied Physics* 114(12), 124313 (2013).
- [27] Liu, C.-C., Nealey, P. F., Ting, Y.-H. and Wendt, A. E., “Pattern transfer using poly(styrene-block-methyl methacrylate) copolymer films and reactive ion etching,” *J. Vac. Sci. Technol. B* 25(6), 1963 (2007).
- [28] Hopf, C., Schlüter, M., Schwarz-Selinger, T., Toussaint, U. von and Jacob, W., “Chemical sputtering of carbon films by simultaneous irradiation with argon ions and molecular oxygen,” *New J. Phys.* 10(9), 93022 (2008).
- [29] Standaert, T., Matuso, P. J. and Li, X., Oehrlein, G.S., “High-density plasma patterning of low dielectric constant polymers: A comparison between polytetrafluoroethylene, parylene-N, and poly(arylene ether),” *Journal of Vacuum Science & Technology A: Vacuum, Surfaces, and Films* 19(2) (2001).
- [30] Belen, R. J., Gomez, S., Kiehlbauch, M. and Aydil, E. S., “In situ measurement of the ion incidence angle dependence of the ion-enhanced etching yield in plasma reactors,” *Journal of Vacuum Science & Technology A: Vacuum, Surfaces, and Films* 24(6), 2176–2186 (2006).
- [31] Ishchuk, V., Olynick, D. L., Liu, Z. and Rangelow, I. W., “Profile simulation model for sub-50 nm cryogenic etching of silicon using SF<sub>6</sub>/O<sub>2</sub> inductively coupled plasma,” *Journal of Applied Physics* 118(5), 53302 (2015).
- [32] Otmar Ertl. and Siegfried Selberherr, “Three-Dimensional Topography Simulation Using Advanced Level Set and Ray Tracing Methods. SISPAD 2008 : September 9-11, 2008, Yumoto Fujiya Hotel, Hakone, Japan,” *IEEE* (2008).
- [33] Choudhary, G. K., Végh, J. J. and Graves, D. B., “Molecular dynamics simulations of oxygen-containing polymer sputtering and the Ohnishi parameter,” *J. Phys. D: Appl. Phys.* 42(24), 242001 (2009).